Polarization effects in Fabry-Pérot interferometer-based solar spectrometers

H.-P. Doerr, O. von der Lühe and T. J. Kentischer

Kiepenheuer-Institut für Sonnenphysik, Schöneckstraße 6, 79104 Freiburg, Germany

ABSTRACT

The influence of thin film multilayer coatings of Fabry-Pérot interferometers (FPI) on polarimetric measurements is investigated. Because the oblique ray reflectivity of the coatings in general is polarization dependent, the transmission profile is slightly different for the *s*- and *p*-components of light passing through the FPI, resulting in weak artificial polarization signals. The difference increases with larger angles of incidence and higher design reflectivity of the coatings. In order to estimate the magnitude of the effect, we perform numerical calculations with different coating designs and different optical configurations. We conclude that while current slow focal ratio solar FPI spectrometers are safe, high-precision polarimetric measurements with large aperture solar telescopes which may require considerably steeper focal ratios may suffer from spurious polarization effects.

Keywords: spectroscopy, polarimetry, Fabry-Pérot interferometer

1. INTRODUCTION

Solar spectrometers based on Fabry-Pérot interferometers (FPI) produce two-dimensional images of the solar surface in very narrow spectral bands which can be tuned to scan absorption lines in the solar spectrum. Combined with a polarization modulator and analyzer, such a spectrometer can perform Stokes polarimetry for investigations of the magnetic field in the solar atmosphere. Typical requirements on the precision with which polarized intensity is to be measured range from one part in 10^3 to 10^4.

Fabry-Pérot etalons are known to produce varying point spread functions across their transmission profile, when used in a telecentric configuration,[1] and to have a field dependent transmission profile in a collimated configuration. Both effects arise from the dependence of the transmission profile on the angle of incidence of a ray on the interferometer. In addition to a wavelength shift, oblique rays should experience a dependence of the transmission on the state of polarization, which to our knowledge has not been studied up to now. In a telecentric mount, differential polarization across the transmission profile of an etalon could produce spurious polarimetric signal in the presence of intensity and polarization gradients with wavelength. Spurious field dependent polarization could be the result for etalons in a collimated configuration. These effects should increase with increasing numerical aperture of the beam at the interferometer.

We extend previous analyses, which are based on a scalar description of the electromagnetic field, to include the full electromagnetic vector in order to understand the effects of Fresnel refraction and reflection in the interferometer on the polarimetric signal and the resulting limitations on polarimetric accuracy. The effect of high-reflectance multilayer coatings on the polarimetric performance is investigated.

Further author information:
E-mail: {doerr, ovdluhe, tk}@kis.uni-freiburg.de, Telephone: +49 (0)761 3198-0

We explore the limits on numerical aperture with respect to polarimetric accuracy for spectrometers which are designed for future large aperture solar telescopes, where Fabry-Pérot etalons pose severe limits on optical throughput and the focal ratio should be as steep as possible. The results of numerical calculations of ideal Fabry-Pérot etalons with different coating designs are presented, and it is found that the influence of the FPI on the polarimetric signal can be neglected in most cases. However, a better understanding of polarization-effects could affect the design of future high-precision filtergraphs such as the *Visible Tunable Filtergraph* (VTF) for the upcoming *Advanced Technology Solar Telescope* (ATST).

2. THEORY

We use the Jones-Calculus to represent polarized light and polarizing optical instruments. Since it is based on the electric field, it allows to calculate interference effects by the coherent superposition of plane waves. This is correct if the single waves propagate parallel to the z-direction, in other cases projection effects must be considered. We are only dealing with comparatively small beam divergences, the minimum f-ratio in this consideration is $f/D = 28$, where f is the focal length and D the diameter of the entrance aperture of the instrument. Therefore, the assumption of parallel propagation is still adequate.

In the Jones calculus, the instantaneous electric field $\mathbf{E}$ of a polarized plane wave traveling along the z-axis is represented by the Jones vector[4]

$$\mathbf{J} := \mathbf{E} = \begin{bmatrix} E_{x,0}\, e^{i\delta_x} \\ E_{y,0}\, e^{i\delta_y} \end{bmatrix}, \tag{1}$$

which contains the initial amplitudes of its orthogonal components $E_{x,0}$ and $E_{y,0}$ and their corresponding phases δ_x and δ_y. The polarization of the wave is then defined by the ratio $\rho = \frac{|E_x|}{|E_y|}$ of its amplitudes and their relative phase difference $\Delta = \delta_x - \delta_y$. Optical devices like polarizers, retarders etc. are represented as 2×2 Jones matrices and the transmitted Jones vector of such a device is found by multiplying the incident Jones vector with the Jones matrix of the device. The total intensity of a Jones vector is proportional to the sum of its squared amplitudes of the x- and y-components. For this study we are not interested in absolute intensities but only in intensity differences, so that the pre-factor can be neglected and the intensity I of a Jones vector $\mathbf{J}$ is

$$I = |J_x|^2 + |J_y|^2 = E_{x,0}^2 + E_{y,0}^2. \tag{2}$$

2.1 Dielectric thin-film multilayers

The Fresnel equations and Snell's law are used to handle reflection and transmission of electromagnetic waves at planar interfaces between homogeneous and isotropic media with different complex refractive indices N_0 and N_1. The complex refractive index is defined as[2]

$$N = n - i\kappa \tag{3}$$

where n is the common index of refraction and κ the extinction coefficient of the medium. κ is zero in transparent media and non-zero in absorbing media. Snell's law connects the angle of incidence ϕ_0 to the angle ϕ_1 of the refracted beam in the second medium by

$$N_0 \sin\phi_o = N_1 \sin\phi_1. \tag{4}$$

Dielectric thin-film coatings consist of many thin dielectric layers, i.e. the layer thickness is in the range of the coherence length of the light so that interference effects occur. Accordingly a "thick" layer is thicker than the coherence length of the light.[2] The transmission and reflection coefficients of the whole multilayer can be calculated from its *characteristic matrix*. A detailed description of the method can be found in, for example, the book by Macleod,[2] which we will summarize shortly in the following.

Consider a multilayer structure as in Fig. 1. The plane of incidence is spanned by the wave vectors of the incident wave and the normal vector of the interface. p and s denote the components of the electric field vibrating parallel and perpendicular to the plane of incidence. The layers are deposited on a substrate medium which is thick, so that back reflections from the substrate into the multilayer can be neglected. The layers are

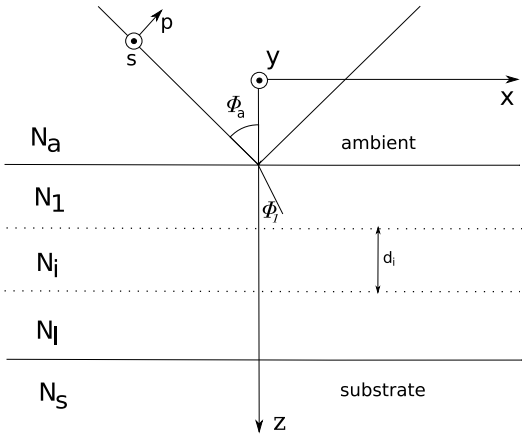

Figure 1. A thin-film multilayer stack.

numbered 1..l, where the first layer adjoins the ambient medium (usually air) and the last layer adjoins the substrate medium. The characteristic matrix $\hat{\mathbf{C}}_i$ of the layer i then relates the tangential components of the electromagnetic field at the interface $i+1$ to the field-components on the interface i

$$\begin{bmatrix} E_i \\ H_i \end{bmatrix} = \begin{bmatrix} \cos\delta_i & i\sin\delta_i/\eta_i \\ i\eta_i\sin\delta_i & \cos\delta_i \end{bmatrix} \begin{bmatrix} E_{i+1} \\ H_{i+1} \end{bmatrix} = \hat{\mathbf{C}}_i \begin{bmatrix} E_{i+1} \\ H_{i+1} \end{bmatrix}, \tag{5}$$

where E and H are the components of the electric and magnetic field amplitudes. $\delta_i = \frac{2\pi}{\lambda} N_i d_i \cos\phi_i$ is the phase shift of a wave after traveling the distance d_i through layer i with the refractive index N_i. η_i is the optical admittance as defined by $\eta_i = N\cos\phi_i$ for the s-polarization and $\eta_i = N/\cos\phi_i$ for the p-polarization. The angle ϕ_i inside the layer can be calculated by repeated application of Snell's law.

The characteristic matrix of a stack of l layers is given by

$$\begin{bmatrix} B \\ C \end{bmatrix} = \left(\prod_{i=1}^{l} \hat{\mathbf{C}}_i \right) \begin{bmatrix} 1 \\ \eta_s \end{bmatrix}, \tag{6}$$

where η_s is the admittance of the substrate and B and C are the total electric and magnetic field components at the interface to the ambient medium as in Eq. (5). The intensity reflection and transmission coefficients of the stack are now calculated from

$$R = \left(\frac{\eta_a B - C}{\eta_a B + C} \right) \left(\frac{\eta_a B - C}{\eta_a B + C} \right)^* \tag{7}$$

and

$$T = \frac{4\eta_a \mathrm{Re}(\eta_s)}{(\eta_a B + C)\,(\eta_a B + C)^*} \tag{8}$$

where η_a is the admittance of the ambient medium. From the conservation of energy, it follows that $R+T+A = 1$, where the absorptance A is zero in dielectric media.

2.2 Fabry-Pérot interferometers

A Fabry-Pérot etalon is an optical resonator made of two planar mirrors of defined spacing d (compare Fig. 2). When a wave enters the etalon from the left side it is reflected multiple times between the inner surfaces of the etalon. At each surface, a fraction r of the amplitude is reflected and a fraction t is transmitted, where r and t are the complex amplitude reflection and transmission coefficients of the coatings.

The amplitude transmittance of a Fabry-Pérot cavity is defined as the ratio of the transmitted and incident complex field amplitudes and is given by[3]

$$\tau(\lambda,\phi) = \frac{E_t}{E_i} = \frac{t_1 t_2}{1 - r_1 r_2 e^{i\Delta(\lambda,\,\phi)}} = \frac{T}{1 - Re^{i\Delta(\lambda,\,\phi)}}, \tag{9}$$

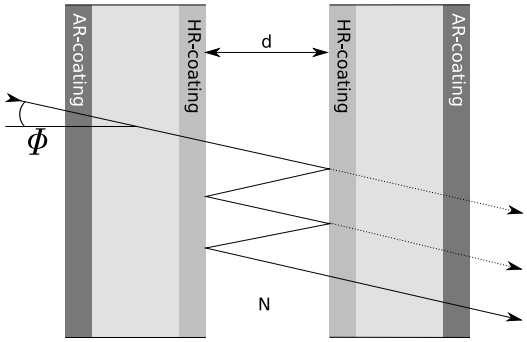

Figure 2. Sketch of a Fabry-Pérot etalon. The etalon plates are plane and parallel and have a spacing d. The outer surfaces are usually coated with an anti-reflection coating, while the inner surfaces have high-reflection coatings.

where λ is the wavelength and ϕ the angle of incidence of the ingoing wave, and $r_{1,2}$, $t_{1,2}$ are the complex amplitude reflection and transmission coefficients of the two etalon plates. We assume the coatings to be identical so that $t_1 = t_2 = t$ and $r_1 = r_2 = r$. $T = |t|^2$ and $R = |r|^2$ are then the intensity transmission and reflection coefficients of the etalon plates. The phase delay a wave experiences while traveling back and forth between the etalon plates is given by

$$\Delta(\lambda,\, \phi) = \frac{2\pi}{\lambda} 2N(d + \epsilon)\cos\phi, \tag{10}$$

where N is the complex refractive index of the medium between the etalon plates, d is the etalon spacing and ϵ a tuning parameter used to match the exact etalon spacing to the desired center wavelength. The intensity reflection and transmission coefficients in Eq. (9) suppress information on the phase, but in this investigation we are only interested in the field amplitudes and not in the phase. The known Airy-formula for the intensity transmission is the square of Eq. (9):

$$I_t(\lambda,\, \phi) = I_0 \frac{T^2}{\left|1 - R\mathrm{e}^{i\Delta(\lambda,\, \phi)}\right|^2}. \tag{11}$$

The reflection and transmission coefficients in Eq. (9) are themselves functions of λ and ϕ and are calculated for each wavelength and angle of incidence by Eqs. (7) and (8). From Eqs. (9) and (10) it follows that for transparent materials and for wavelengths matching the cavity spacing, the transmittance of a FPI is unity, regardless of the reflectivity of the etalon mirrors. But for any wave that does not fulfill the resonance condition ($\Delta = n\pi$, where n is an integer), the transmittance becomes a function of the R and T coefficients of the etalon so that the polarization of these waves will be altered.

For the p and s components, Eq. (9) can be expressed as a matrix

$$\begin{bmatrix} \frac{T_p}{1 - R_p\mathrm{e}^{i\Delta(\lambda,\, \phi)}} & 0 \\ 0 & \frac{T_s}{1 - R_s\mathrm{e}^{i\Delta(\lambda,\, \phi)}} \end{bmatrix}, \tag{12}$$

which contains the amplitude transmission coefficients of the FPI for the p and s polarization components. The local p and s components at the plane-of-incidence are related to the global x and y coordinates of the Jones coordinate system by a rotation by the azimuthal angle ϑ (Fig. 3). The rotation matrix $\hat{\mathbf{R}}_\pm$ is therefore

$$\begin{bmatrix} p \\ s \end{bmatrix} = \begin{bmatrix} \cos(\vartheta) & \sin(\vartheta) \\ -\sin(\vartheta) & \cos(\vartheta) \end{bmatrix} \begin{bmatrix} x \\ y \end{bmatrix} = \hat{\mathbf{R}}_+ \begin{bmatrix} x \\ y \end{bmatrix} \tag{13}$$

where the index $\pm$ denotes forward or backward rotation. The Jones matrix of a Fabry-Pérot interferometer is then

$$\hat{\mathbf{M}}_{\mathrm{FPI}} = \hat{\mathbf{R}}_- \begin{bmatrix} \tau_p(\phi,\, \lambda) & 0 \\ 0 & \tau_s(\phi,\, \lambda) \end{bmatrix} \hat{\mathbf{R}}_+. \tag{14}$$

Eq. (14) only respects the internal reflections inside the Fabry-Pérot cavity, neglecting any effects when the wave

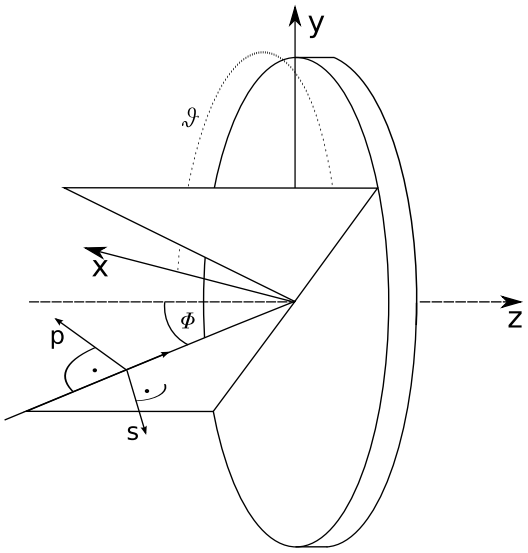

Figure 3. Plane of incidence on the Fabry-Pérot interferometer. The local p, s-system and the global x, y-system are rotated by an azimuthal angle ϑ. If $\vartheta = 0$ and the angle of incidence ϕ is very small, s is parallel to y and p is parallel to$x$.

enters the FPI through the first etalon plate, and leaves it through the second plate. Because of the high number of internal reflections in contrast to only two transmission processes, this simplification seems appropriate.

The change of polarization upon reflection and transmission can be expressed by the ratios of the complex reflection and transmission coefficients

$$\begin{aligned} \rho_r =& \frac{r_p}{r_s} = \tan\Psi\, \mathrm{e}^{i\Delta_r} \\ \rho_t =& \frac{t_p}{t_s} = \tan\Psi\, \mathrm{e}^{i\Delta_t}, \end{aligned} \tag{15}$$

where $\Delta = \delta_p - \delta_s$ are the relative phase shifts for both components upon reflection or transmission. Eq. (15) is the fundamental equation of ellipsometry, and Δ and Ψ are the two *ellipsometric angles*. The values of Δ and Ψ can be measured by an ellipsometer or polarimeter.[4]

While the ratios of the amplitudes exponentiate with higher number of reflections, the change in phase is linear because $r = a\mathrm{e}^{i\delta}$ and thus, $r^n = a^n \mathrm{e}^{in\delta}$, where a is the amplitude of the reflection coefficient r, and δ its phase factor. In this paper, we will restrict the research on the amplitude.

2.2.1 Telecentric vs. collimated mount

The intensity distribution in the focal plane resulting from the light of a point source entering the instrument, is called the point spread function (PSF). The PSF of an ideal instrument is basically the Fourier transform of the entrance aperture, often also referred to as the entrance pupil. The PSF limits the spatial resolution and its shape characterizes the imaging quality of an instrument.

From Eqs. (9) and (10) it follows that the transmission maximum of the FPI shifts towards the blue for increasing angles of incidence ϕ. The relative shift in wavelength for small angles is given by[1]

$$\Delta\lambda = \lambda \frac{\phi^2}{2N}, \tag{16}$$

where N is the refractive index of the medium between the etalon plates. The consequences of this blue shift with respect to the imaging quality of the instrument depend on the position of the FPI within the optical path. In the so called *telecentric* mount (see below) it leads to a *pupil apodisation*, a radial variation in the pupil illumination in the presence of spectral gradients in the incoming light. The pupil apodisation leads to varying

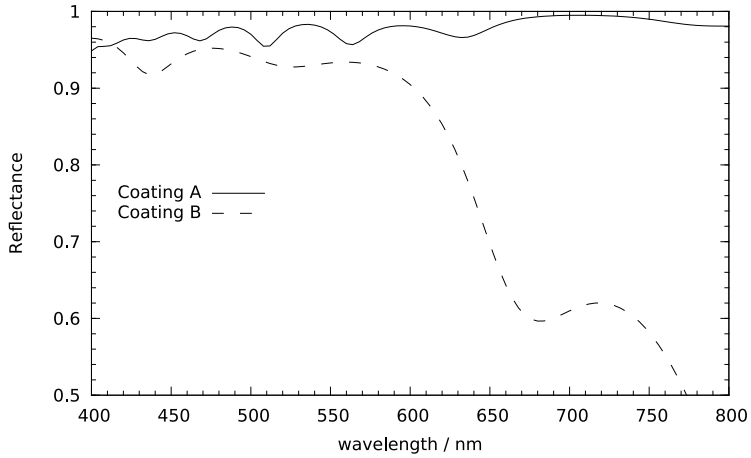

Figure 4. The calculated reflection curves for the two coating designs A and B used in the simulations.

PSFs when the FPI is tuned over a spectral line. This effect was already discussed by Beckers,[1] von der Lühe and Kentischer[5] and Scharmer.[6] It was found that the problems of the telecentric mount can be suppressed when the f-ratio of the optical path is large enough ($f/D > 200$). The pupil apodisation could also affect polarimetric measurements, but this is not in the scope of this paper. Here, we will focus on the intrinsic polarization of the Fabry-Pérot cavity.

In the telecentric mount the FPI is located at the focal plane and the pupil is collimated through the FPI. Each ray emerging from the pupil propagates under a different angle through the FPI, resulting in a radial polarization gradient through the pupil when seen from behind the FPI. In the *collimated* mount the FPI is located at the pupil plane and the focal plane is collimated through the FPI. Each ray emerging from the focal plane propagates under a different angle through the FPI, resulting in a radial polarization gradient through the focal plane when seen from behind the FPI.

3. NUMERICAL SIMULATIONS

While a qualitative discussion of the polarization effect can be derived by discussing the properties of the Airy-formula Eq. (11) in dependence of the values of R and T, quantitative predictions require numerical simulations. The calculation of the reflection and transmission coefficients of a multilayer structure would be a very elaborately task without the help of computers. In order to investigate the magnitude of the change in polarization as discussed above, we implemented the methods described in the previous sections in a numerical code written in the C language. The code calculates the amplitude of the electric field in the pupil plane resulting from a polarized plane wave entering the instrument under a certain angle of incidence. From the pupil field, the focal plane field is calculated via a discrete Fourier transfrom (DFT) which, for a point-source, is identical to the PSF of the system. The change in the amplitude components of the wave is then the difference of the ratios ρ_r and ρ_t as defined in Eq. (15) before and after passing the interferometer. To simulate polychromatic light, we incoherently summarize the intensity fields of monochromatic calculations over the passband of the FPI.

To compare the effect of different coatings, we use two examples of broad band high reflection coatings from the book by Macleod.[2] The reflectance curves for these two coatings A and B are shown in Fig. 4. Design A is a 21 layer stack made of ZnS and Cryolite, design B is a 13 layer stack which is made of ZnS, Cryolite, $PbCl_2$ and MgF_2.

The following calculations were performed with a plate separation of the etalon of 1.0 mm, resulting in a free spectral range (FSR) of about 1.25 Å at a reference wavelength λ_0 of 500 nm. The FWHM depends on the reflectance of the coatings. At λ_0 it is 12.2 mÅ for the FPI with coating A and 24.2 mÅ for the FPI with coating B, in the following referred to as FPI A and FPI B. To keep things simple, the incoming light was linearly polarized at 45 degrees and of equal intensity at each wavelength.

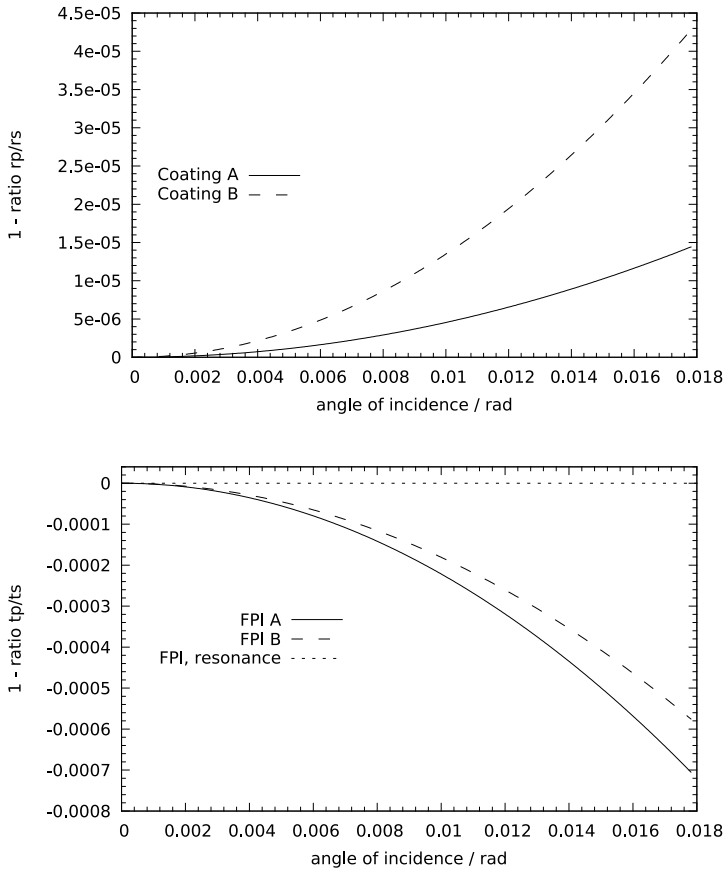

Figure 5. Ratios of the amplitude reflection coefficients of the plain coating (upper figure), and the ratios of the effective amplitude transmission coefficients of FPI A and FPI B (lower figure). The maximum angle of incidence corresponds to a f-ratio of $f/D = 28$ and a wavelength shift of about 80 pm towards the blue.

We first calculated the ratios $\frac{|r_p|}{|r_s|}$ for the plain coatings, and $\frac{|t_p|}{|t_s|}$ for the transmission coefficients of the FPIs as a function of the angle of incidence. Fig. 5 shows the results for the plain coatings and for FPI A and B. For convenience, we plotted the deviation of the ratios from one. The wavelength of the incoming light for each angle of incidence was chosen such that it is shifted by -10 mÅ relative to the optimal transmission wavelength as of Eq. (16). For the optimal transmission wavelength, the difference of the transmission coefficients is zero, as shown by the dotted curve in Fig. 5. The plain coating A introduces less polarization from a single reflection than coating B. This becomes different for the performance of the whole FPI, where FPI A introduces more polarization. This is due to the higher reflectivity of coating A and the resulting higher number of internal reflections.

So far we only used monochromatic plane waves. As soon as we introduce polychromatic light, we will face partial polarization wich can no longer be handled by means of the Jones calculus. Instead we synthesize intensity profiles by integrating the monochromatic intensities of the transmitted amplitudes over the passband of the FPI

$$I(\lambda_c) = \int_{-\infty}^{+\infty} |E_i(\lambda)\, \tau_{\lambda_c}(\lambda)|^2 \, \mathrm{d}\lambda, \tag{17}$$

where $\tau_{\lambda_c}(\lambda)$ is the amplitude transmittance of a FPI tuned to the center wavelength λ_c and for a wavelength λ of the incident wave. E_i is the amplitude of the incident wave. For the numerical integration of Eq. (17), we set the integration limits $\lambda_c \pm \delta\lambda$ to those wavelengths, where the transmission profile Eq. (11) dropped to 10^{-5} of

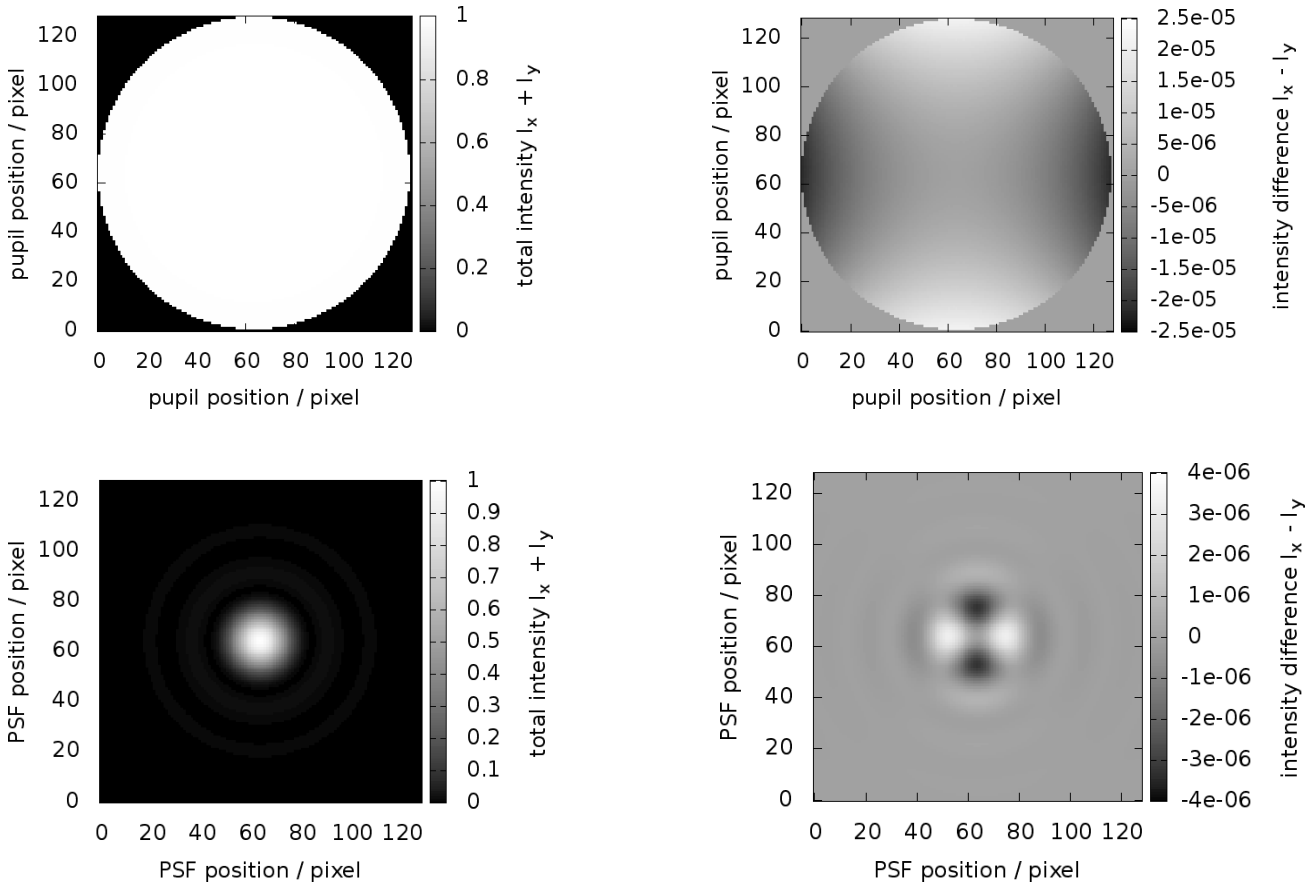

Figure 6. Calculated polychromatic pupil illumination (upper left) and resulting PSF (lower left) and the corresponding difference of the x and y intensity components of FPI A in a $f/128$ beam.

the value at the center wavelength

$$I(\lambda_c) = \Delta\lambda \sum_{\lambda=\lambda_c-\delta\lambda}^{\lambda=\lambda_c+\delta\lambda} \left| E_i(\lambda)\, \tau_{\lambda_c}(\lambda) \right|^2 , \tag{18}$$

where $\Delta\lambda$ is the sampling interval of the wavelength.

The differences of the normalized intensities for the x and y component can be interpreted as an Stokes Q signal.[4] The following two-dimensional calculations were done on a 2048×2048 pixel grid, where the pupil had a diameter of 128 pixels so that the PSF resulted in a reasonable size. The FPI was tuned to the reference wavelength of $\lambda_c = 500\,\mathrm{nm}$.

The first column of Fig. 6 shows the calculated total intensity distribution in the pupil plane and the corresponding PSF of FPI A in a telecentric mount. The second column shows the differences of the intensities of the x and y components in the pupil and PSF. Horizontal cross sections through the pupil and the core of the PSF are shown in Fig. 7. While the difference of the intensities is up to 2.5×10^{-5} at the pupil edge, the maximum difference of the PSF is only some 10^{-6} which is way below the stated requirement on polarimetric accuracy of up to 10^{-4}

For the same settings as above, but with a f-ratio of $f/D = 28$, a similar calculation was performed. The results are shown in Fig. 8. Here, both components differ by about 10^{-4} in the pupil and 10^{-5} in the PSF. The calculations for FPI B, which are not shown here, look quite similar.

Finally, we calculated the PSF of FPI A in a collimated mount at different angles of incidence, i.e. at different positions in the field of view (FOV). The maximum angle of incidence is $\phi_{max} = 0.00391$ rad which corresponds

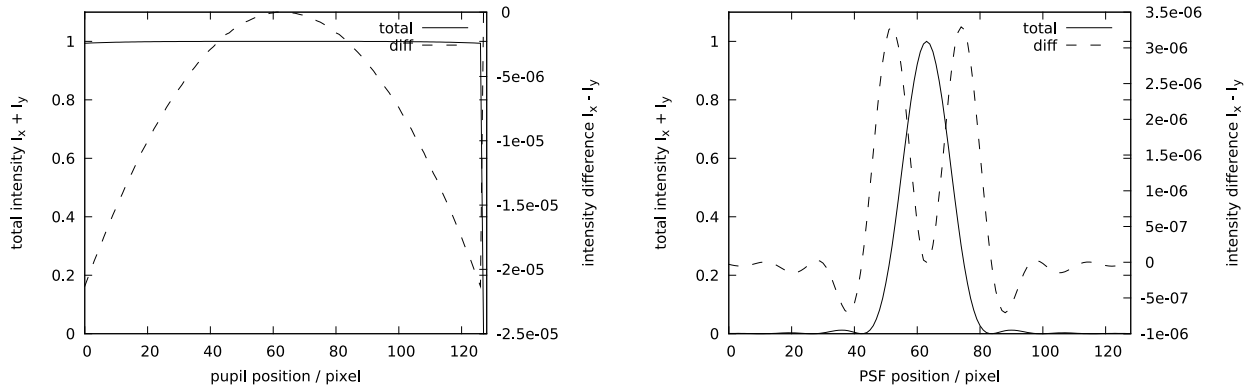

Figure 7. Horizontal cross sections of the pupil and the PSF of FPI A in a $f/128$ beam.

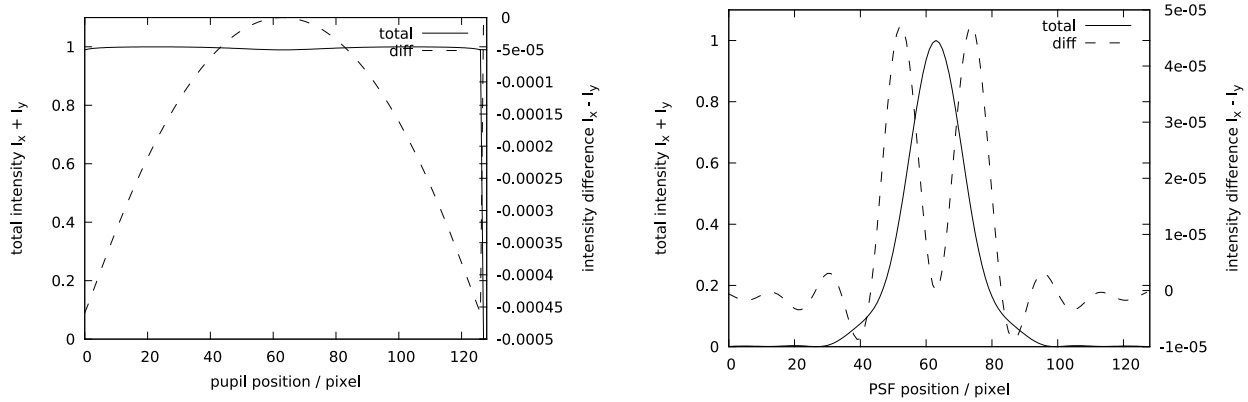

Figure 8. Horizontal cross sections of the pupil and the PSF of FPI A in a $f/28$ beam.

to the edge of the FOV in a $f/128$ beam. Both components are equal at normal incidence, as shown on the left side of Fig. 9. At oblique incidence, the difference is proportional to the total intensity with a maximum of 4.5×10^{-5} at the edge of the FOV.

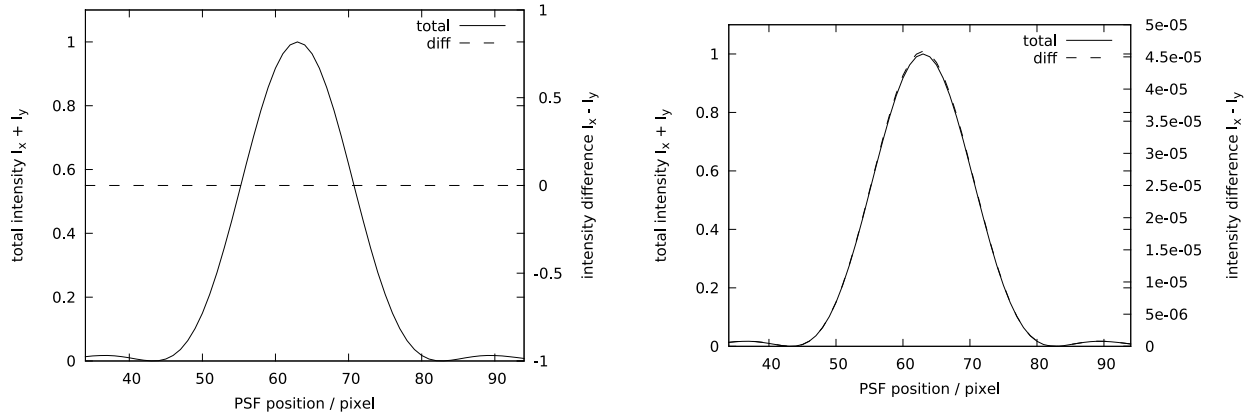

Figure 9. Cross sections of the PSF of FPI A in a collimated $f/128$ beam at normal incidence (left) and maximum oblique incidence (right).

4. CONCLUSIONS

A Fabry-Pérot interferometer alters the polarization of light when it enters the FPI with an oblique angle, for wavelengths which do not fulfill the resonance condition. As a consequence, spurious polarization signal may arise in the presence of field and wavelength dependent gradients of intensity. The effect increases with the angle of incidence, but is sufficiently small in beams with slow f-ratios to be safely disregarded in solar Fabry-Pérot spectrometers which are currently in use. Our analyses indicate that steeper focal ratios, which may become necessary for future large-aperture solar telescopes, require consideration of polarization effects if the interferometer is to be used for high precision polarimetry. Further analyses as well as experiments are under way to conclude this question.

REFERENCES

[1] Beckers, J. M., "On the effect of narrow-band filters on the diffraction limited resolution of astronomical telescopes," *Astron. Astrophys. Suppl. Ser.* **129**, 191–194 (Apr. 1998).

[2] Macleod, H. A., [*Thin-Film Optical Filters*], Institute of Physics Publishing, Bristol and Philadelphia, 3. ed. (2001).

[3] Vaughan, J., [*The Fabry-Pérot Interferometer*], Institute of Physics Publishing, Bristol and Philadelphia (1989).

[4] Azzam, R. and Bashara, N., [*Ellipsometry and Polarized Light*], North-Holland Publishing Company, Amsterdam, New York and Oxford, 1. ed. (1979).

[5] von der Lühe, O. and Kentischer, T. J., "High spatial resolution performance of a triple Fabry-Pérot filtergraph," *Astron. Astrophys. Suppl. Ser.* **146**, 499–506 (Nov. 2000).

[6] Scharmer, G. B., "Comments on the optimization of high resolution Fabry-Pérot filtergraphs," *Astron. Astrophys.* **447**, 1111–1120 (Mar. 2006).